EXTENDED EXPERIMENTAL PROCEDURES

Antibodies and Peptides

Antibodies to following antigens were used: Lck (clone 3A5), VAV (rabbit polyclonal), SLP76 (rabbit polyclonal, all Santa Cruz Biotechnology); Erk1/2 (clone L34F12), ZAP70 (clone L1E5), Erk1/2 pT202/pY204 (clone D13.14.4E), ZAP70 pY319 (rabbit), Src family pY416 (rabbit), Src family non-pY416 (mouse, clone 7G9, all Cell Signaling); TCRζ pY142 (clone K25-407.69) (all BD Biosciences); LAT pY191 (rabbit polyclonal), pTyrosine (clone 4G10, both Merck Millipore); actin (rabbit polyclonal, Sigma-Aldrich); CD3ε (clone 145-2C11), CD8α (clone 53-6.7), CD8β (clone 53-5.8), CD4 (clones RM4-5 and H129.19), TCRβ (clone H57-597), TCR-Vα2 (clone B20.1), CD69 (clone H1.2F3) (all BD PharMingen). For flow cytometry, antibodies were conjugated to various fluorescent dyes by the manufacturer.

Determination of Surface Molecule Numbers

Saturating concentrations of PE–conjugated antibodies were determined (40 μg/ml for CD3ε, CD8α and 10 μg/ml for CD4). 25,000 cells were stained in 25 μl of staining buffer (PBS/2% FCS) for 40 min on ice, washed, and analyzed along with PE calibration beads (RCP-30-5A, Spherotech Inc., Lake Forest, IL, USA) by flow cytometry. A calibration curve was generated based on the fluorescence signal from calibration beads to transform the geometric mean of fluorescence intensity (after subtraction of background signal from antibody stained peripheral B cells) into mean equivalent of PE intensity (MEPE) values. The actual number of surface molecules was calculated by adjusting the MEPE values to the PE/antibody ratio (determined by absorbance at 560 nm using soluble PE as a standard). Number of antigens captured by one molecule of antibody was assumed to be 2 (Davis et al., 1998), except for TCR, where the results were further corrected for the presence of 2 CD3ε molecules per TCR/CD3 complex.

Flow Cytometric Immunoprecipitation Assay

10^6 cells were lysed in 50 μl lysis buffer (1% NP-40, 10 mM Tris pH 7.4, 140 mM NaCl, 2 mM EDTA, Protease Inhibitor Cocktail (Sigma-Aldrich)) for 30 min on ice. 75,000 CML beads (Invitrogen) coupled to anti-CD4 (clone RM4.4), anti-CD8β (clone 53-5.8), or anti-MHCI (clone Y3.8) antibodies, as described previously (Schrum et al., 2007), were added to the lysate and incubated for 3 hr at 4°C. Beads were washed 3x in lysis buffer and stained with different PE-conjugated antibodies to CD4 (clone H129.19), CD8α (clone 53-6.7), or Lck (clone 3A5) at saturating concentrations (40 min, on ice) and analyzed by flow cytometry. The geometric mean fluorescence intensities (gMFI) were taken as the measure of the antibody binding. The CD8, CD8.4 or CD4-Lck coupling ratio was calculated as Lck signal to CD8 or CD4 signal (after subtracting respective background signal measured from control anti-MHCI beads) and adjusted for the PE/antibody ratio.

Calcium Mobilization

Cells (10^7/ml in RPMI/10%FCS) were loaded with 0.5 μM Indo-1 (Invitrogen) for 30 min at 37°C. Calcium mobilization was measured as a ratio of Indo-1 fluorescence intensities elicited by emission wavelengths at 400–500 nm and 500–560 nm (excitation 355 nm). Baseline Ca^{2+} mobilization was determined for 30 s after which, cells were stimulated by addition of 2 × concentrated activators (tetramers or ionomycin in RPMI/10%FCS). Measurements were continued for 5 min. Calcium response index (Stepanek et al., 2011) was calculated as the percentage of cells with an intracelluar calcium level, higher than the 90^{th} percentile found in resting cells during a 10 s time interval prior to stimulation.

Mice

B3K506 Rag1$^{-/-}$ I-A$^{-/-}$ and B3K508 Rag1$^{-/-}$ I-A$^{-/-}$ mice were generated by breeding B3K506 Rag1$^{-/-}$ and B3K508 Rag1$^{-/-}$ with I-A$^{-/-}$ mice.

Cells

The OT-I hybridoma line expressing CD8β-YFP and TCRζ-CFP (Mallaun et al., 2008), and T2-K^b cells (a gift from T. Potter) were cultivated in RPMI/10% FBS, 100 U/ml penicillin, 100 μg/ml streptomycin, and 50 μM 2-mercapthoethanol.

Cell Stimulation

DP thymocytes (2 × 10^8 mil/ml) were preincubated in RPMI (10 min, 37°C) and stimulated by adding an equal volume of 200 nM tetramers in RPMI. At indicated time points, cells were either fixed in formaldehyde (intracellular staining) or lysed in 2x SDS PAGE sample buffer (western blotting).

CD69 Upregulation Assay

T2-Kb cells were pre-incubated with varying amounts of peptide for 2 hr before addition of thymocytes. Final concentrations were 6 × 10^5 T2Kb cells, 10^6 thymocytes, and indicated concentration of peptide in 250 μl of RPMI/10% FCS. Thymocytes were examined by flow cytometry 24 hr later, using antibodies to CD69, CD4, CD8α, and Vα2 TCR. The EC_{50} values for CD69 upregulation were calculated using nonlinear regression curve (y = a+(b-a)/(1+10^((log(EC_{50})-x) × H))). Aggregate data showing CD8WT/CD8.4 EC_{50} versus CD8WT EC_{50} dependency were fitted with log-log line regression (y = 10^(a × log(x)+b)).

Determination of Lck Phosphorylation Status

Preselection OT-I thymocytes were either treated with 20 μM PP2 (Calbiochem) or 1 mM pervanadate for 10 min or left untreated. Cells were lysed in a lysis buffer (1% dodecylmaltoside, 1 mM Pefabloc, 5 mM iodoacetamide, 1mM sodium orthovanadate, 100 mM NaCl, 50 mM NaF, 10% glycerol v/v, and 20 mM Tris, pH 7.5) and incubated for 30 min on ice. Nuclei and debris were removed by centrifugation, and the resulting lysate was subjected to immunoprecipitation with anti-Lck antibody (2 μg/ml) followed by incubation with Protein G Sepharose (GE Healthcare). Immunoprecipitates were eluted with SDS-PAGE sample buffer and subjected to immunoblotting. Src family pY416 and Src family non-pY416 antibodies were used for the detection of the phosphorylation state of Lck Y394. Signals from phospho and non-phospho specific antibodies were normalized to total Lck signal. The percentage of phosphorylated Lck in untreated cells (P) was calculated using equation:

$$P = \frac{\frac{b_2}{b_1} - 1}{\frac{b_2}{b_1} - \frac{a_2}{a_1}}$$

where *b* and *a* are signal intensities from non-phospho and phospho specific antibodies, respectively (Stepanek et al., 2011). The terms 1 and 2 represent untreated and treated conditions, respectively. Percentage of phosphorylated Lck was independently calculated using either PP2 or PV-treated cells and averaged to obtain a single value for each independent experiment.

Generation of Expression Plasmids

The OT-I TCR α and β chains, H2-K^b heavy chain and human β2 m chain were generated by PCR mutagenesis (Stratagene) and PCR cloning. Three versions of the OT-I TCR were generated. One with a leucine zipper attached to the C terminus, one with a biotinylation site on the alpha chain C terminus, and one incorporating human constant domains with an artificial inter chain disulphide to produce the soluble TCR. These molecules contained residues 1–207 and 1–247 of TCRα and β, respectively (Boulter et al., 2003; Garboczi et al., 1996). H2-K^b heavy chain (residues 1–248) (α1, α2 and α3 domains), tagged with a biotinylation sequence, and human β2 m (residues 1–100) were also cloned and used to generate pMHCI complexes. The TCR α and β chains, the H2-K^b α chain and human β2 m sequences were inserted into separate pGMT7 expression plasmids under the control of the T7 promoter (Garboczi et al., 1996).

Protein Expression, Refolding, Purification

Competent Rosetta DE3 *E.coli* cells were used to produce the TCR α and β chains, H2-K^b heavy chain and human β2 m in the form of inclusion bodies following induction with 0.5 mM IPTG as described previously (Cole et al., 2006, 2008; Garboczi et al., 1996). Biotinylated pMHCI was prepared as previously described (Wyer et al., 1999).

MHC Tetramer and Monomer-Qdot Assembly

K^b-peptide and I-A^b-peptide tetramers were generated by incubating biotinylated pMHC monomers with streptavidin (Jackson Immunoresearch) or PE-streptavidin (Invitrogen) at a 4:1 ratio on ice. Streptavidin was separately added to pMHC-monomers in two aliquots. Qdot-labeled pMHC monomers were generated by mixing biotinylated pMHC monomers with Qdot605-streptavidin conjugates (Invitrogen) at a 0.5:1 ratio for 20 min at 26°C. Free biotin binding sites were subsequently blocked with an excess of free biotin.

Surface Plasmon Resonance

SPR equilibrium binding analysis was performed using a BIAcore T100™ equipped with a CM5 sensor chip as previously reported (Cole et al., 2007; Gostick et al., 2007; Wyer et al., 1999). Experiments were conducted with H2-K^b variants immobilised on the chip surface. Two OT-I TCR constructs, one with a leucine zipper attached to the C terminus and one implementing a human constant domain with an artificial inter chain disulphide, were used in different experiments. SPR equilibrium analyses were carried out to determine the K_D values for OT-I:H2-K^b-APL interactions at 25°C in multiple experiments (representative data shown). In all experiments, approximately 300 response units of pMHC or TCR were coupled to the CM5 sensor chip surface. Analyte was injected at concentrations ranging from 10 times above and 10 times below the known K_D of the interaction (where possible) at 45 μl/min. K_D values were calculated assuming 1:1 Langmuir binding ($AB = B^*AB_{MAX}/(K_D + B)$) and data were analyzed using a global fit algorithm (BIAevaluation™ 3.1). A blank flow cell and irrelevant HLA-A*0201-ALWGPDPAAA, or HLA-B*3501-VPLRPMTY monomers were used as negative controls on flow cell 1. The SPR measurements for B3K506 and B3K508 TCRs were carried out previously at 25°C (Huseby et al., 2006).

Single Molecule Microscopy

LabTek chambers (Thermo Scientific) were precoated with poly-l-lysine at 37°C overnight. 1–2 × 10^6 lymph node T cells or thymocytes were stained with anti-CD45.2-AlexaFluor488 antibody, washed and resuspended in 200 μl of RPMI (without phenol red)/5% FCS and added to the chamber. Cells were allowed to attach to the surface for at least 30 min. A Nikon A1 microscope equipped with 100 × magnifying objective (1.49Na), ORCA2 CCD camera (Hamatsu Photonics), and Visiview software (Visitron systems) were used to acquire images using 50 ms exposure time. One frame consisted of 14 Z-steps with a track radius of 0.65 μm collected over 0.7 s.

3D movies were analyzed using Imaris software (Bitplane). The measurements of the Qdot-pMHC dwell times on the cell surface were done manually, excluding first three and last three frames of each movie. Only binding events, which began and ended during the time of the movie and lasted at least 2 frames, were analyzed. The number of persisting binding events was ploted versus time and fitted with to a one phase exponential decay function: $Y = Y_{max} \times e^{-\ln 2 \times X/\tau 1/2}$.

Statistical Analysis

Curve fitting and statistical analysis was performed using Prism version 5.0d (GraphPad Software) and Excel for Mac 2011 version 14.3.9 (Microsoft).

Markov Chain Model

To model the interactions between an engaged TCR (TCR-pMHC) and CD4 or CD8 coreceptors in the membrane, we generated a Markov chain model (Figure 6A). The interactions of CD4 and CD8 with Lck seem to be very strong, because the majority of Lck molecules in thymocytes are bound to CD4 or CD8 coreceptors (Van Laethem et al., 2007; Van Laethem et al., 2013). In contrast, the CD4 or CD8 interactions with MHCII or MHCI, respectively, are rather weak and transient (Gao and Jakobsen, 2000; Wyer et al., 1999). For our model, we assumed that the CD4- and CD8-Lck interactions are stable and there is negligible Lck turnover among the coreceptors within the time scale of interest (<30 s). In this context, DP thymocytes contain a small fraction of Lck-coupled coreceptors and a larger pool of empty coreceptors, devoid of Lck (Figure 2). We neglected the role of coreceptor-free Lck in TCR triggering for two reasons, because it comprises less than 1/3 of total Lck in thymocytes (Van Laethem et al., 2007). Moreover, a significant part of the coreceptor-free pool is not anchored in the plasma membrane and cannot easily contribute to TCR signaling. (Zimmermann et al., 2010). While a free Lck molecule within the cytoplasm might occasionally collide with a TCR, this occurs in a random orientation and presumably has a only a small chance to phosphorylate CD3 and ZAP70. In contrast, coreceptor-bound Lck is recruited to the TCR complex in a more constrained position under the plasma membrane. In this regard, it has been postulated that orientation of a coreceptor-bound Lck is constrained to optimize phosphorylation of CD3 chains (Li et al., 2013). This gives an advantage to coreceptor-bound Lck.

The model predicts that the TCR-pMHC (TM) pair typically scans multiple coreceptor molecules before it encounters one coupled with Lck.

The parameters for the Markov chain models are listed in Table S2. For the case of calculations, we considered that there is just one TCR-pMHC pair and a proportional number of coreceptors (= C/A, ca. 3500 in case of CD8) on a 1 μm × 1 μm patch of membrane. The average distance between the TCR-pMHC and a coreceptor molecule is:

$$r = \frac{1}{\sqrt{\pi \times C/A}} \qquad \text{(Equation 1)}$$

The average time for a TM to form a pair (close proximity) with a coreceptor is:

$$\tau = \frac{r^2}{D} \qquad \text{(Equation 2)}$$

Thus, the k_{f0} and k_{f1} finding rates for forming a pair with a coreceptor loaded with (active) Lck (TM+LC) or with a coreceptor devoid of (active) Lck (TM+C), respectively, are:

$$k_{f0} = \frac{1}{\tau_0} = \frac{(1-f)\pi CD}{A} \qquad \text{(Equation 3)}$$

$$k_{f1} = \frac{1}{\tau_1} = \frac{f\pi CD}{A} \qquad \text{(Equation 4)}$$

We assumed a lattice spacing of l = 0.01 μm, meaning that when a coreceptor and TCR-pMHC are in the same lattice site, they can either diffuse apart or bind with rates k_d and k_b, respectively. The diffusion coefficient was scaled to a "hopping rate" k_d, that describes the movement of molecules in the lattice grid:

$$k_d = \frac{D}{l^2} \qquad \text{(Equation 5)}$$

The initial state of the Markov chain is a free TCR-pMHC (TM) and the formation of coreceptor-Lck:TCR-pMHC complex was set as an absorbing end state. A set of 5 ordinary differential equations describe the evolution of probabilities of the various states of the model with time (see also Figure 6A):

$$\frac{dP_{TM:C}}{dt} = -k_u P_{TM:C} + k_b P_{TM+C} \qquad \text{(Equation 6)}$$

$$\frac{dP_{TM+C}}{dt} = k_u P_{TM:C} - (k_d + k_b) P_{TM+C} + k_{f0} P_{TM} \quad \text{(Equation 7)}$$

$$\frac{dP_{TM}}{dt} = k_d (P_{TM+C} + P_{TM+LC}) - (k_{f0} + k_{f1}) P_{TM} \quad \text{(Equation 8)}$$

$$\frac{dP_{TM+LC}}{dt} = k_{f1} P_{TM} - (k_d + k_b) P_{TM+LC} \quad \text{(Equation 9)}$$

$$\frac{dP_{TM:LC}}{dt} = k_b P_{TM+LC} \quad \text{(Equation 10)}$$

These equations were numerically solved (f = 0.014, for other parameters see Table S2 - CD8), showing that the TCR/pMHC mainly exists as a TM+C pair or eventually in the absorbing LC:TM state shortly after the initial time of TCR-pMHC binding (Figure S5D).

One of the most difficult parameters to estimate was k_u, the off-rate of coreceptor:MHC interaction. For CD8, we took the SPR data from human CD8αα interaction with HLA-2 (Wyer et al., 1999). The authors determined the dissociation rate to be $\geq$ 18 s^{-1}. Because other studies measured a higher CD8:MHCI affinity in the mouse system (indicating slower off-rate) we used k_u = 20 s^{-1} (close to the lower value) in the model. The affinity of CD4:MHCII interaction is lower than the affinity CD8-MHCI interaction, but association and dissociation rates of CD4:MHC binding and unbinding are above the detection limit of SPR (Gao and Jakobsen, 2000; van der Merwe and Davis, 2003; Xiong et al., 2001). We assumed a similar on-rate for both coreceptors (Artyomov et al., 2010), but a 10-fold higher off-rate for CD4-MHCII (200 s^{-1}). We experimentally determined the number of CD4, CD8, and TCR molecules on preselection DP thymocytes (Figures S5A and S5B) and diffusion coefficients for CD8 (0.085 μm^2 s^{-1}) and TCR (0.13 μm^2 s^{-1}) in a hybridoma cell line (Figure S5C). Others reported slightly lower diffusion coefficient for TCR (ca. 0.05–0.06 μm^2 s^{-1}) in primary T cells (Dushek et al., 2008). Based on our and previously published data, we assumed a diffusion coefficient of 0.08 μm^2 s^{-1} for both TCR and CD8. Remaining parameters were taken from the relevant literature or estimated (Table S2) (Altan-Bonnet and Germain, 2005; Artyomov et al., 2010).

Equations describing the Markov state model were solved using MATLAB (MathWorks). We also tested some results of the Markov state model with fully stochastic solutions of the Master equations (data not shown) using a numerical implementation of the Gillespie method, called Stochastic Simulation Compiler (Lis et al., 2009). The probabilities of Lck delivery to the TCR as a function of time were generated for CD4 (MHCII), CD8 (MHCI), and CD8.4 (MHCI) coreceptors using numerical solution of the Markov chain model (Figure 6B).

Approximate Analytical Solution of the Reduced Markov Chain Model

To obtain an approximate analytical solution, we simplified the Markov chain model. Because we saw that the TM+C and TM+LC pairs are very infrequent and short-lived (Figure S5D) and approximately constant during the simulation (not shown), we made a pseudo-steady state assumption and set Equations 7 and 9 to 0. The free TM state is very short-lived, because it rapidly encounters a coreceptor. Thus, we assumed that the initial state of the model is TM:C ($P_{TM:C}(0) = 1$; $P_{TM:LC}(0) = 0$) and extended the pseudo-steady state to the free state (TM) as well. The simplified model consisted of the following equations (Equations 11, 12, 13, 14, and 15):

$$\frac{dP_{TM:C}}{dt} = -k_u P_{TM:C} + k_b P_{TM+C} \quad \text{(Equation 11)}$$

$$\frac{dP_{TM+C}}{dt} = k_u P_{TM:C} - (k_d + k_b) P_{TM+C} + k_{f0} P_{TM} = 0 \quad \text{(Equation 12)}$$

$$\frac{dP_{TM}}{dt} = k_d (P_{TM+C} + P_{TM+LC}) - (k_{f0} + k_{f1}) P_{TM} = 0 \quad \text{(Equation 13)}$$

$$\frac{dP_{TM+LC}}{dt} = k_{f1} P_{TM} - (k_d + k_b) P_{TM+LC} = 0 \quad \text{(Equation 14)}$$

$$\frac{dP_{TM:LC}}{dt} = k_b P_{TM+LC} \quad \text{(Equation 15)}$$

The analytical solution of the reduced model is:

$$P_{TM:C}(t) = e^{-\lambda t};\ P_{TM:LC}(t) = 1 - e^{-\lambda t} \quad \text{(Equation 16)}$$

Where λ is the rate of TCR-pMHC:Lck collision mediated by coreceptors.

$$\lambda = \frac{k_d k_{f1} k_u}{(k_b + k_d)(k_{f0} + k_{f1})} = \frac{fDk_u}{D + l^2 k_b} \quad \text{(Equation 17)}$$

The approximate analytical solution showed very similar results to the numerical solution of the full model (not shown).

TCR Occupancy Model

The TCR occupancy model assumes that the number of TCRs occupied by pMHC ligands determines the signal generated in a T cell or thymocyte. The magnitude of the response (R) can be calculated as:

$$R = TCR_{oc} = \frac{\frac{L}{A} + \frac{T}{A} + \frac{ln2}{k_{on} \times \tau_{1/2}} - \sqrt{\left(\frac{L}{A} + \frac{T}{A} + \frac{ln2}{k_{on} \times \tau_{1/2}}\right)^2 - \frac{4LT}{A^2}}}{2} \times A \quad \text{(Equation 18)}$$

where TCR_{oc} is the number of occupied TCRs in an equilibrium, k_{on} is 2D on-rate of the ligand (Huppa et al., 2010), L and T are numbers of ligands and TCRs, respectively, in the T cell/APC interface, and $\tau_{1/2}$ is the half dwell time of the TCR-pMHC interaction. We estimated the contact area between the thymocyte and APC to be one third of the total thymocyte surface.

"Lck Come&Stay/Signal Duration Model"

This model postulates that a TCR signal begins once a TCR-pMHC pair binds a coreceptor loaded with (active) Lck and the Lck-mediated phosphorylation results in recruitment and phosphorylation of ZAP70. The recruited coreceptor-Lck complex stays catalytically active for the duration of TCR-pMHC binding and generates additional down-stream signals by maintaining the ZAP70 in the active state. To calculate the TCR response in this scenario, we combined the Lck recruitment rate with the model of kinetic proofreading (McKeithan, 1995), that takes into account the Lck catalytic rate and the number of Lck-mediated phosphorylations required for ZAP70 recruitment and activation:

$$R = TCR_{oc} \times \frac{\lambda}{\lambda + k_{off}} \times \left(\frac{k_p}{k_p + k_{off}}\right)^n \quad \text{(Equation 19)}$$

where k_{off} is off-rate of the ligand (= $ln2/\tau_{1/2}$), k_p is the Lck catalytic rate, and n is the number of Lck-mediated phosphorylations of TCRζ and ZAP70 required to trigger the TCR (i.e., activate TCR-bound ZAP70). The magnitude of the induced TCR response (R) is determined by the number of triggered and still occupied TCRs at (pseudo)equilibrium. When accounting for TCR occupancy, the equation expands to:

$$R = \frac{\frac{L}{A} + \frac{T}{A} + \frac{ln2}{k_{on} \times \tau_{1/2}} - \sqrt{\left(\frac{L}{A} + \frac{T}{A} + \frac{ln2}{k_{on} \times \tau_{1/2}}\right)^2 - \frac{4LT}{A^2}}}{2} \times A \times \frac{\lambda}{\lambda + k_{off}} \times \left(\frac{k_p}{k_p + k_{off}}\right)^n \quad \text{(Equation 20)}$$

Because positive selectors do not induce a true synapse formation, the decision to proceed toward negative selection must be made before the synapse is formed (Ebert et al., 2008; Melichar et al., 2013). For this reason, the 'Lck come&stay/signal duration' model does not assume any significant accumulation of TCRs (nor pMHC) in the thymocyte-APC interface. The parameters are summarized in Table S3 (Huppa et al., 2010; Ramer et al., 1991).

Since it was previously shown in two independent reports that negative selection can be induced when 2–3 high-affinity antigen molecules are present at the thymocyte/APC interface (Ebert et al., 2008; Peterson et al., 1999), we used this experimental observation as an assumption in our model; i.e., to initiate negative election, $\geq$ 2–3 TCRs must be continuously activated up to the point of generating catalytically active ZAP70 within 5 min. The 5min interval was taken from the observations of Robey et al., who showed that in the absence of cognate antigen, thymocytes interact with an APC for an average of ~5 min (Melichar et al., 2013).

"Lck Come&Stay/Serial Triggering Model"

This model differs from the 'Lck come&stay/signal duration model' by assuming that once a TCR has been triggered by Lck-mediated activation of ZAP70, there is no further increase in the amount of TCR signal generated by continued ligand occupancy. Thus, short dwelling ligands benefit because they can trigger additional TCRs or have more attempts to trigger at least one TCR, while long dwelling ligands are arrested on TCRs that have already been fully triggered. In this model, the magnitude of the induced TCR response (R)

is expressed as a number of TCRs triggered during a time interval (length of a thymocyte-APC interaction before a decision is made) and can be calculated as:

$$R = \frac{\frac{L}{A}+\frac{T}{A}+\frac{ln2}{k_{on}\times\tau_{1/2}} - \sqrt{\left(\frac{L}{A}+\frac{T}{A}+\frac{ln2}{k_{on}\times\tau_{1/2}}\right)^2 - \frac{4LT}{A^2}}}{2} \times A \times \frac{\lambda}{\lambda+k_{off}} \times \left(\frac{k_p}{k_p+k_{off}}\right)^n \times t \times k_{off} \quad \text{(Equation 21)}$$

Model of Multiple Lck Visits

This model postulates that repetitive Lck visits are required for TCR triggering. We assumed that an Lck-coupled coreceptor remains at the TCR/pMHC complex just long enough to enable a single phosphorylation of the TCRζ or a recruited ZAP70 molecule. Thus, accumulation of n Lck visits within the dwell time of TCR/pMHC engagement would eventually lead to the TCR triggering. This model can be combined with the signal duration model, where the magnitude of the induced TCR response (R) is expressed as a number of triggered and occupied TCRs in equilibrium:

$$R = \frac{\frac{L}{A}+\frac{T}{A}+\frac{ln2}{k_{on}\times\tau_{1/2}} - \sqrt{\left(\frac{L}{A}+\frac{T}{A}+\frac{ln2}{k_{on}\times\tau_{1/2}}\right)^2 - \frac{4LT}{A^2}}}{2} \times A \times \left(\frac{\lambda}{\lambda+k_{off}}\right)^n \quad \text{(Equation 22)}$$

or with the serial triggering model, where the magnitude of the induced TCR response (R) is expressed as a number of TCRs triggered during a time interval:

$$R = \frac{\frac{L}{A}+\frac{T}{A}+\frac{ln2}{k_{on}\times\tau_{1/2}} - \sqrt{\left(\frac{L}{A}+\frac{T}{A}+\frac{ln2}{k_{on}\times\tau_{1/2}}\right)^2 - \frac{4LT}{A^2}}}{2} \times A \times \left(\frac{\lambda}{\lambda+k_{off}}\right)^n \times t \times k_{off} \quad \text{(Equation 23)}$$

SUPPLEMENTAL REFERENCES

Alam, S.M., Davies, G.M., Lin, C.M., Zal, T., Nasholds, W., Jameson, S.C., Hogquist, K.A., Gascoigne, N.R., and Travers, P.J. (1999). Qualitative and quantitative differences in T cell receptor binding of agonist and antagonist ligands. Immunity *10*, 227–237.

Altan-Bonnet, G., and Germain, R.N. (2005). Modeling T cell antigen discrimination based on feedback control of digital ERK responses. PLoS Biol. *3*, e356.

Boulter, J.M., Glick, M., Todorov, P.T., Baston, E., Sami, M., Rizkallah, P., and Jakobsen, B.K. (2003). Stable, soluble T-cell receptor molecules for crystallization and therapeutics. Protein Eng. *16*, 707–711.

Cole, D.K., Rizkallah, P.J., Gao, F., Watson, N.I., Boulter, J.M., Bell, J.I., Sami, M., Gao, G.F., and Jakobsen, B.K. (2006). Crystal structure of HLA-A*2402 complexed with a telomerase peptide. Eur. J. Immunol. *36*, 170–179.

Cole, D.K., Rizkallah, P.J., Boulter, J.M., Sami, M., Vuidepot, A.L., Glick, M., Gao, F., Bell, J.I., Jakobsen, B.K., and Gao, G.F. (2007). Computational design and crystal structure of an enhanced affinity mutant human CD8 alphaalpha coreceptor. Proteins *67*, 65–74.

Cole, D.K., Dunn, S.M., Sami, M., Boulter, J.M., Jakobsen, B.K., and Sewell, A.K. (2008). T cell receptor engagement of peptide-major histocompatibility complex class I does not modify CD8 binding. Mol. Immunol. *45*, 2700–2709.

Davis, K.A., Abrams, B., Iyer, S.B., Hoffman, R.A., and Bishop, J.E. (1998). Determination of CD4 antigen density on cells: role of antibody valency, avidity, clones, and conjugation. Cytometry *33*, 197–205.

Dushek, O., Mueller, S., Soubies, S., Depoil, D., Caramalho, I., Coombs, D., and Valitutti, S. (2008). Effects of intracellular calcium and actin cytoskeleton on TCR mobility measured by fluorescence recovery. PLoS ONE *3*, e3913.

Gao, G.F., and Jakobsen, B.K. (2000). Molecular interactions of coreceptor CD8 and MHC class I: the molecular basis for functional coordination with the T-cell receptor. Immunol. Today *21*, 630–636.

Garboczi, D.N., Ghosh, P., Utz, U., Fan, Q.R., Biddison, W.E., and Wiley, D.C. (1996). Structure of the complex between human T-cell receptor, viral peptide and HLA-A2. Nature *384*, 134–141.

Gostick, E., Cole, D.K., Hutchinson, S.L., Wooldridge, L., Tafuro, S., Laugel, B., Lissina, A., Oxenius, A., Boulter, J.M., Price, D.A., and Sewell, A.K. (2007). Functional and biophysical characterization of an HLA-A*6801-restricted HIV-specific T cell receptor. Eur. J. Immunol. *37*, 479–486.

Li, Y., Yin, Y., and Mariuzza, R.A. (2013). Structural and biophysical insights into the role of CD4 and CD8 in T cell activation. Front. Immunol. *4*, 206.

Lis, M., Artyomov, M.N., Devadas, S., and Chakraborty, A.K. (2009). Efficient stochastic simulation of reaction-diffusion processes via direct compilation. Bioinformatics *25*, 2289–2291.

Mallaun, M., Naeher, D., Daniels, M.A., Yachi, P.P., Hausmann, B., Luescher, I.F., Gascoigne, N.R., and Palmer, E. (2008). The T cell receptor's alpha-chain connecting peptide motif promotes close approximation of the CD8 coreceptor allowing efficient signal initiation. J. Immunol. *180*, 8211–8221.

Ramer, S.E., Winkler, D.G., Carrera, A., Roberts, T.M., and Walsh, C.T. (1991). Purification and initial characterization of the lymphoid-cell protein-tyrosine kinase p56lck from a baculovirus expression system. Proc. Natl. Acad. Sci. USA *88*, 6254–6258.

Rosette, C., Werlen, G., Daniels, M.A., Holman, P.O., Alam, S.M., Travers, P.J., Gascoigne, N.R., Palmer, E., and Jameson, S.C. (2001). The impact of duration versus extent of TCR occupancy on T cell activation: a revision of the kinetic proofreading model. Immunity *15*, 59–70.

van der Merwe, P.A., and Davis, S.J. (2003). Molecular interactions mediating T cell antigen recognition. Annu. Rev. Immunol. *21*, 659–684.

Wyer, J.R., Willcox, B.E., Gao, G.F., Gerth, U.C., Davis, S.J., Bell, J.I., van der Merwe, P.A., and Jakobsen, B.K. (1999). T cell receptor and coreceptor CD8 alphaalpha bind peptide-MHC independently and with distinct kinetics. Immunity *10*, 219–225.

Xiong, Y., Kern, P., Chang, H., and Reinherz, E. (2001). T Cell Receptor Binding to a pMHCII Ligand Is Kinetically Distinct from and Independent of CD4. J. Biol. Chem. *276*, 5659–5667.

Zimmermann, L., Paster, W., Weghuber, J., Eckerstorfer, P., Stockinger, H., and Schütz, G.J. (2010). Direct observation and quantitative analysis of Lck exchange between plasma membrane and cytosol in living T cells. J. Biol. Chem. *285*, 6063–6070.

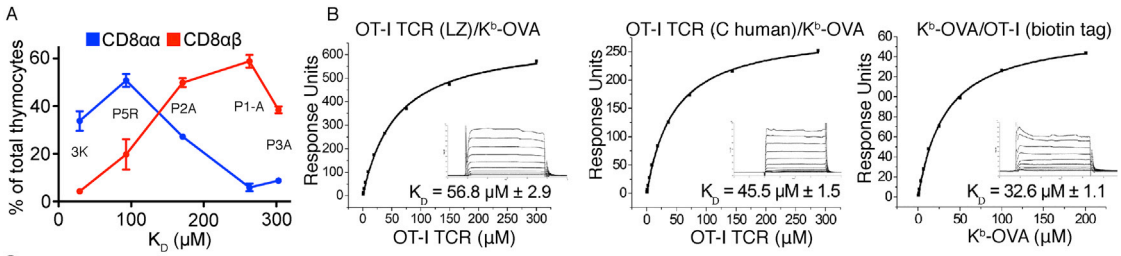

C

Analyte injected over immobilised ligand	OT-I TCR Leucine zipper at C-terminus		OT-I TCR C human interchain artificial disulphide		K^b-OVA, prep 2
Ligand immobilised onto chip surface	K^b-OVA, prep1	K^b-OVA, prep 2	K^b-OVA, prep1	K^b-OVA, prep 2	OT-I TCR (biotin tag)
Exp 1 BIA 3000	46.1 μM ± 3	39.0 μM ± 6	66.3 μM ± 5	46.6 μM ± 6	ND
Exp 2 BIA T100	38.9 μM ± 2	55.4 μM ± 1	45.5 μM ± 2	61.4 μM ± 2	ND
Exp 3 BIA T100	56.8 μM ± 3	50.5 μM ± 3	ND	ND	32.6 μM ± 1

D

	Peptide	OVA	Q4R7	T4	Q7	Q4H7	V4	G4	R4	E4
Exp1	K_D (μM)	50.5 ± 2.7	268.3 ± 31.1	578.4 ± 38.9	628.0 ± 42.8	834.7 ± 56.6	>1mM	>1mM	ND	NB
Exp2	K_D (μM)	56.8 ± 2.9	307.4 ± 12.3	310 .1 ± 51.5	488.4 ± 35.3	858.8 ± 118.6	ND	ND	>1mM	ND
Mean	K_D (μM)	54	288	444	558	847	>1mM	>1mM	>1mM	NB

Figure S1. SPR Affinity Measurements, Related to Figure 1

(A) Relative frequency of CD8αα and CD8αβ thymocytes in B3K508 FTOCs (see Figure 1A). Mean ± range, n = 2. CD8αα cells appeared under conditions of negative selection and thus, probably represent a nonconventional innate-like T cell lineage (Yamagata et al., 2004). In contrast, a population of CD8αβ SPs were generated in FTOCs exposed to positive selecting ligands; these cells are either immature single positive thymocytes, a transitional stage between double negative and double positive cells or a population of thymocytes undergoing an atypical positive selection fate; this has been previously described for thymocytes expressing another MHCII-restricted TCR, 5C.C7 (Yamagata et al., 2004).

(B and C) Ten serial dilutions of OT-I TCR were measured in multiple experiments using different TCR constructs and experimental setups. Representative data from these experiments are plotted and the mean K_D ± SD was calculated. To calculate background binding, OT-I TCR, or H2-K^b–OVA was also injected over a negative control sample that was subtracted from the experimental data. (Left panel) OT-I TCR with a leucine zipper at the C terminus binding to immobilized H2-K^b–OVA. (Middle panel) OT-I TCR with a human C terminus binding to immobilized H2-K^b–OVA. (Right panel) H2-K^b–OVA binding to biotin tagged immobilized OT-I TCR. Two different preparations of H2-K^b-OVA from two different labs gave similar results (EP and AKS).

(D) Ten serial dilutions of OT-I TCR with C-terminal leucine zipper were measured in multiple experiments using different K^b-OVA peptide variants. Mean K_D values ± SD were calculated and are indicated in the table. NB, not binding. ND, not determined. Our SPR affinity measurements of the interaction between OT-I TCR and K^b-OVA or K^b-OVA-derived APLs showed much higher K_D values and a more pronounced difference between strong and weak ligands than previously published SPR data on the same TCR (Alam et al., 1999; Rosette et al., 2001). While Alam et al. (1999) determined the K_D of OT-I/H-2K^b-OVA and OT-I/H-2K^b-E1 (very weak ligand) to be 6 μM and 20 μM, respectively, our measurements showed K_D ~50 μM for K^b-OVA and > 1 mM for ligands even more potent than K^b-E1. We measured two different H-2K^b-OVA preparations produced in two labs and two different OT-I TCR constructs that were heterodimerized using a non-native disulphide bond or a leucine zipper. In different experiments, the soluble TCRs were used as analyte or bait ligand. All experiments produced similar results. As the previous report showed an unexpected decrease in binding dynamics at higher temperature, these data might have been influenced by protein aggregation. The measurements determined in this work correspond more closely with the distribution of antigen potencies of the various OT-I ligands (Daniels et al., 2006). As the previously published data have been frequently used for modeling of the TCR response and for arguing against the relevance of SPR measurements in studying TCR-pMHC interactions, the affinities measured here may resolve some of the discrepancies in the literature.

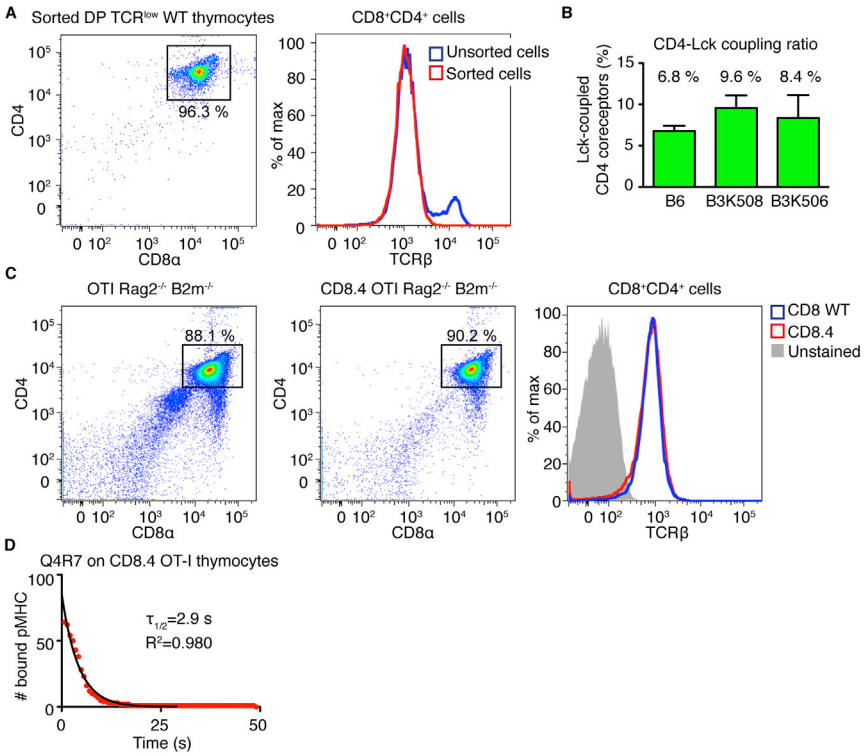

Figure S2. Determining Coreceptor-Lck Coupling, Related to Figure 2

(A) Sorted preselection CD3^{low} DP thymocytes from B6 mice were analyzed for CD4, CD8α, and TCRβ expression levels. Purity of DP thymocytes (left panel) and TCR levels on sorted DP thymocytes compared to unsorted thymocytes (right panel) are shown.

(B) Mean percentage ± SD of Lck-coupled CD4 molecules in B3K506 Rag1$^{-/-}$ I-A$^{-/-}$, B3K508 Rag1$^{-/-}$ I-A$^{-/-}$, and sorted polyclonal DP TCR^{low} thymocytes is shown (n = 2–5).

(C) CD8WT and CD8.4 OT-I DP thymocytes were stained with antibodies to CD4, CD8α, and TCRβ. Percentage of DP thymocytes (left panel) and TCR levels on pre-selection DP thymocytes (right panel) are shown.

(D) On cell dwell times of Q4R7 monomer on CD8.4 OT-I DP thymocytes were measured by single molecule microscopy and fitted using a one phase exponential decay curve; $\tau_{1/2}$ and R-square values are shown. $\tau_{1/2}$ on CD8WT (Figure 1E) and CD8.4 OT-I DP thymocytes are similar.

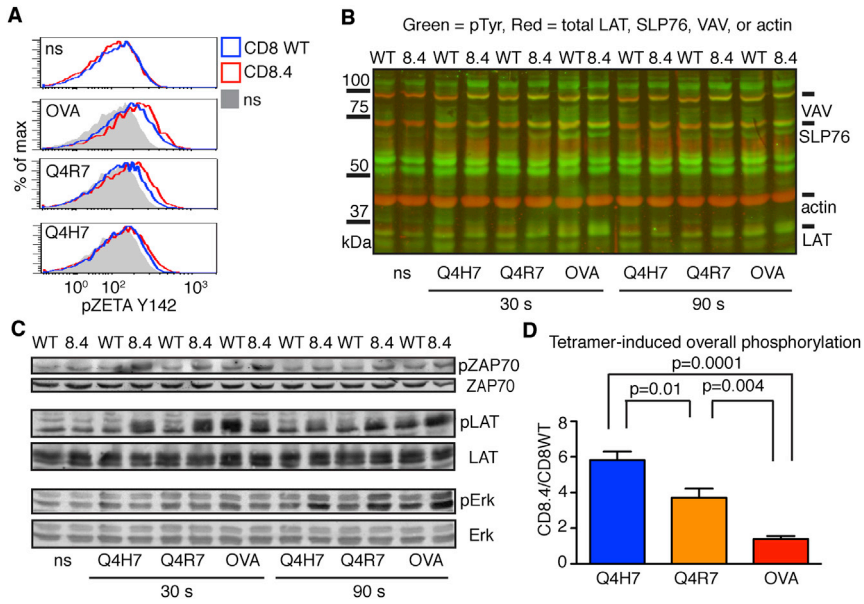

Figure S3. CD8.4 Enhances Proximal Signaling in OTI Thymocytes, Related to Figure 4

Thymocytes from CD8WT and CD8.4 OTI Rag2$^{-/-}$β2 m$^{-/-}$ mice were stimulated with 100 nM K^{b}-OVA, K^{b}-Q4R7, or K^{b}-Q4H7 tetramers or left unstimulated (ns).

(A) Zeta chain phosphorylation was analyzed by flow cytometry. A representative experiment from a total of 6 is shown.

(B) Total phosphorylation of VAV, SLP76, and LAT was analyzed by probing whole cell lysates with mouse anti-pTyr antibody (green) and rabbit antibodies to VAV, SLP76, LAT, and actin (red) by western blotting. A representative experiment from a total of 4 is shown.

(C) The phosphorylation of specific phosphorylation site was analyzed by probing whole cell lysates with antibodies to LAT pY191, ZAP70 pY319, and Erk pT202/Y204 by western blotting. Total ZAP70, LAT, and Erk served as the respective loading controls. A representative experiment from a total of 4 is shown.

(D) Tetramer induced increase of Erk1 (at 90 s), ZAP70, LAT, VAV, and SLP76 (at 30 s) phosphorylation was calculated by subtracting normalized basal level of phosphorylation from the values induced following tetramer stimulation (Figure 4B–4G). For each phosphoprotein, the average ratio of the induced phosphorylation (determined from 4 experiments) observed in CD8.4 and CD8 WT thymocytes was calculated (CD8.4/CD8WT). To obtain a broader view of the differences in early signaling intermediates, the ratios for the induction of the various phosphoproteins were pooled; from these pooled values, the mean and SEM were plotted. Statistical significance was tested using Student's t test (2 tailed, unequal variance).

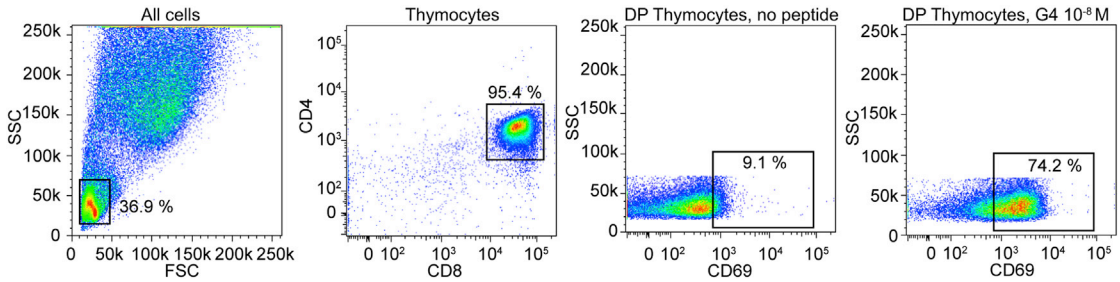

Figure S4. Gating Strategy, Related to Figure 5

CD8WT and CD8.4 OT-I Rag2$^{-/-}$ β2 m$^{-/-}$ thymocytes were incubated with peptide loaded APCs (T2-K^{b} cells) for 24 hr and stained with antibodies to CD4, CD8, and CD69. DP thymocytes were gated using FSC^{low}SSC^{low}/CD4^{+}CD8^{+}. Individual gates are shown.

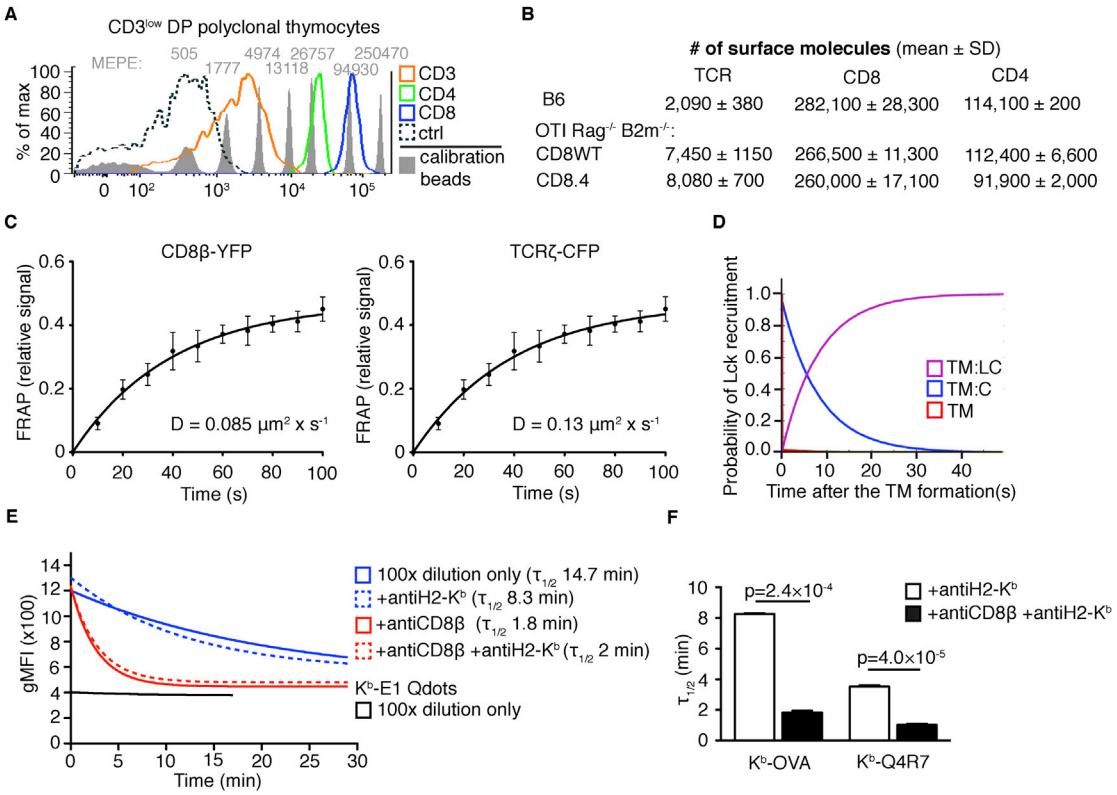

Figure S5. Parameters Relevant to Coreceptor Exchange, Related to Figure 6

(A) Sorted preselection polyclonal TCRβ^{low} DP thymocytes and control cells (peripheral B cells) were stained with saturating concentration of PE-conjugated antibodies to CD4, CD8α, or CD3 and analyzed by flow cytometry together with PE calibration beads. Fluorescence signals from stained thymocytes, negative control (representative negative control for CD3 staining) and calibration beads are shown. The number of mean equivalent soluble PE molecules (MEPE) is indicated for each peak of the PE calibration beads.

(B) Quantification of the number of TCR, CD8, and CD4 molecules per cell (mean number ± SD from 3 experiments) expressed on polyclonal sorted preselection DP thymocytes (B6) as well as CD8WT and CD8.4 OT-I Rag2$^{-/-}$ β2 m$^{-/-}$ thymocytes.

(C) Fluorescence recovery after photobleaching (FRAP) CD8β-YFP and TCRζ-CFP in OT-I hybridoma cell line was performed using an Olympus IX81 inverted microscope. Mean normalized fluorescence recovery ± SD (n = 6 for CD8β, n = 7 for TCRζ). The points were fitted with an exponential equation y = a × (1-e^(-K × x)). Calculated diffusion coefficients are shown.

(D) Probability of various states in the Markov chain model. TM (free TCR-pMHC), TM:C (TCR-pMHC complexed with an Lck-free coreceptor), and TM:LC (TCR-pMHC complexed with an Lck-bound coreceptor) states are shown. The states TM+C and TM+LC (TCR-pMHC in a close proximity of an Lck-free or Lck-bound coreceptor, respectively) are very rare (under the resolution of the y axis).

(E) OT-I preselection thymocytes were incubated with 100 nM monomeric K^b-OVA Qdots or K^b-E1 Qdots in PBS/5% FCS at 4°C for 2 hr to establish binding equilibrium. Subsequently, the cells were diluted 100x with the staining buffer with or without antiCD8β (clone 53.5.8, Biolegend) and/or antiH2-K^b (clone Y3) antibodies (10 μg/ml). The antiH2-K^b antibody was used to prevent antigen rebinding. The decrease of Qdot fluorescence intensity was monitored by flow cytometry at 0°C in real time. K^b-E1 Qdots monomers that have undetectable binding to OT-I TCR were used to determine baseline fluorescence signal. Blocking free CD8 rapidly accelerated the release of antigen from the thymocytes, providing experimental evidence for the cycling of coreceptors at the TCR-pMHC complex, as assumed by our Markov chain model. In contrast, preventing of rebinding of monomers to the thymocytes using anti-H2-K^b antibody had only a modest effect (compare solid and dashed lines). This showed that the effects of CD8 blocking cannot be explained by inhibition of new thymocyte-pMHC interactions due to antigen rebinding. Data were fitted with a one phase exponential decay function.

(F) Quantifying the effect of CD8 blocking on the dissociation of prebound K^b-OVA and K^b-Q4R7 monomers from OT-I T cells. Mean ± SEM n = 2–5. Statistical significance was tested using Student's t test (unequal variance, 2 tailed).

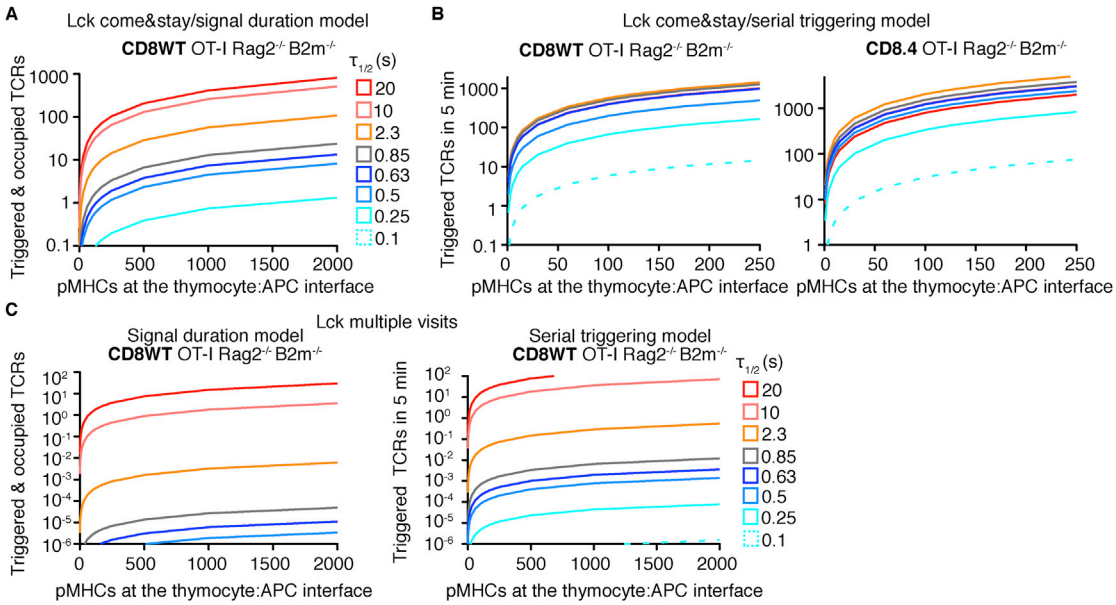

Figure S6. Four Models of TCR Triggering, Related to Figure 7

Graphs show the TCR signal intensity as a function of number of cognate ligands at the thymocyte/APC interface for different ligands (k_{on} = 0.1 $\mu m^2 s^{-1}$, $\tau_{1/2}$ varied).
(A) 'Lck come&stay/signal duration model' as in Figure 7A with x axis scaled up to show the effect of increasing antigen concentration to non-physiological levels.
(B) 'Lck come&stay/serial triggering model' for CD8WT OT-I Rag2$^{-/-}$ β2 m$^{-/-}$ and CD8.4 OT-I Rag2$^{-/-}$ β2 m$^{-/-}$ thymocytes.
(C) 'Multiple Lck visits/signal duration model' and 'Multiple Lck visits/serial triggering model' for CD8WT OT-I Rag2$^{-/-}$ β2 m$^{-/-}$ thymocytes.
See Extended Experimental Procedures.